NUMERICAL ANALYSIS MODELING FOR QUANTITATIVE PREDICTION OF EJECTA DISPERSAL BEHAVIOR DUE TO HYPER-VELOCITY IMPACT

Sho Kajihara[(1)], Souichi Maruyama[(2)], Keisuke Kubota[(2)], Ryo Higuchi[(2)], Tomohiro Yokozeki[(2)], Satomi Kawamoto[(3)], Shinichi Takeda[(3)], Masanori Kobayashi[(4)]

[(1)] Meiji University, 1-1-1 Higashimita Tama-ku Kawasaki Kanagawa 214-8571 Japan, Email: kajihara@meiji.ac.jp
[(2)] The University of Tokyo, 7-3-1 Hongo Bunkyo-ku Tokyo 119-8656 Japan, Email: {omaruso1yen@g.ecc.u-tokyo.ac.jp, kubota-keisuke852@g.ecc.u-tokyo.ac.jp, higuchi@aastr.t.u-tokyo.ac.jp, yokozeki@aastr.t.u-tokyo.ac.jp}
[(3)] Japan Aerospace Exploration Agency, 7-44-1 Jindaiji Higashi-machi Chofu-shi Tokyo 182-8522 Japan, Email: kawamoto.satomi@jaxa.jp
[(3)] Japan Aerospace Exploration Agency, 6-13-1 Osawa Mitaka-shi Tokyo 181-0015 Japan, Email: takeda.shinichi@jaxa.jp
[(4)] Chiba Institute of Technology, 2-17-1 Tsudanuma Narashino-shi Chiba 275-0016 Japan, Email: kobayashi.masanori@it-chiba.ac.jp

ABSTRACT

Under the accelerated development and utilization of space environment, the problem of countermeasures against secondary debris (ejecta) generated by collisions between space structures and space debris / Micrometeoroids and Orbital Debris (MMOD) has become an issue. In this study, the numerical analysis model and prediction scheme for the ejecta to the hyper-velocity impacts were established. As the base study, the 1 mm diameter projectile and rectangular target plate were modelled with particle elements based on the Smoothed Particle Hydrodynamics (SPH) method in LS-DYNA. The materials for the projectile and target were A2024-T3 and A6061-T6, respectively. The Johnson-Cook model for yield stress and failure strain was applied to the SPH model. Linear multinomial equation of state and Mie-Gruneisen equation of state were used, referred to previous studies. To validate the created model, collision tests at velocities of 1, 3, 5, and 7 km/s were performed to quantitatively evaluate ejecta behavior and target crater. The experiment was conducted using a two-stage light gas gun. The copper plates used for ejecta collection, called Witness Plate (WP), were placed on the front and rear sides of the target, respectively. The debris cloud shape, ejecta generation mass, the diameter of the target crater, and the maximum diameters of scars on WP were observed and compared with numerical simulation, showing qualitative consistency. The proposed numerical analysis model could adequately provide the tendency of ejecta increase with velocity and target thickness. The created model was used to predict the ejecta behavior at hypervelocity (> 7km), where collision tests cannot be performed. The results showed that the ejecta size would be dramatically larger than at lower collision velocities.

1 INTRODUCTION

Recently, the increase of space debris has become a big problem with accelerated space utilization. Space debris and Micrometeoroids and Orbital Debris (MMOD) Space debris and Micrometeoroids and Orbital Debris (MMOD) are numerous around the Earth, some with velocities of 10 km/s or more [1, 2]. Then, there is concern that the secondary debris produced by hyper-velocity collisions may cause a chain of subsequent collisions, resulting in a state in which debris self-propagates. The secondary debris is called ejecta, and it is one of the causes of debris increase. A wide range of space projects using large structures such as the Space Solar Power System (SSPS) have been considered, and the probability of collision will increase. Especially, space debris accumulates at high altitudes, such as the geostationary orbit (GEO), where purification by atmospheric resistance cannot be expected. From those backgrounds, prediction of ejecta dispersal behavior and structural materials that can suppress ejecta are required.

Many collision tests have been conducted in previous studies [3, 4]. However, experiments have limitations such as impact velocity, specimen size, and high cost. As described above, space debris collides at ultrahigh speeds exceeding 10 km/s, making it difficult to reproduce the collision in experiments. On the other hand, numerical analysis has no such limitations. Therefore, the authors established a numerical analysis model and prediction scheme for the ejecta behavior of aluminum to the hyper-velocity impacts.

In this study, a numerical model on aluminum debris collisions is constructed, and the validity of the model is verified through a quantitative comparison of ejecta behavior with experimental results in the 1~7 km/s (high velocity) range. Furthermore, using the constructed model, we will perform analysis in the ultra-

Proc. 9th European Conference on Space Debris, Bonn, Germany, 1–4 April 2025, published by the ESA Space Debris Office
Editors: S. Lemmens, T. Flohrer & F. Schmitz, (http://conference.sdo.esoc.esa.int, April 2025)

high velocity range where experiments are not possible, describe the characteristics observed in ultra-high velocity collisions, and estimate the amount and size of ejecta generated.

2 NUMERICAL ANALYSIS MODEL

In this study, numerical analysis was performed using the Smoothed Particle Hydrodynamics (SPH) method. The SPH method is a method for approximating the motion of a continuum by discretizing it as a collection of a finite number of particles and considering the motion of individual particles. Since it does not require any mesh, it has the advantage of being suitable for problems involving large deformations. The numerical model was established in LS-DYNA, as shown in Fig. 1. The projectile size was set to 1 mm diameter in the numerical simulation and collision test described below. The target was a square plate with 20 mm length and t (= 1, 2, 4) [mm] thickness. The projectile model and target plate model are composed of particles with a 0.05 mm distance. The dependence of the number of particles on the simulation results was investigated in advance, and it was confirmed that the results converged at this particle spacing. The four edges of the upper and lower surfaces of the target are completely fixed as boundary conditions. The spherical projectile was given an initial velocity V in the negative direction of the Z-axis and collided with the target.

The materials used in this study were A6061-T6 for the target plate and A2024-T3 for the projectile. Their properties are summarized in Tab. 1. The Johnson-Cook model [5] was adopted for them because the Johnson-Cook model can consider the large strain, high temperature, and high pressure associated with high strain rates and have been well used for hyper velocity impact.

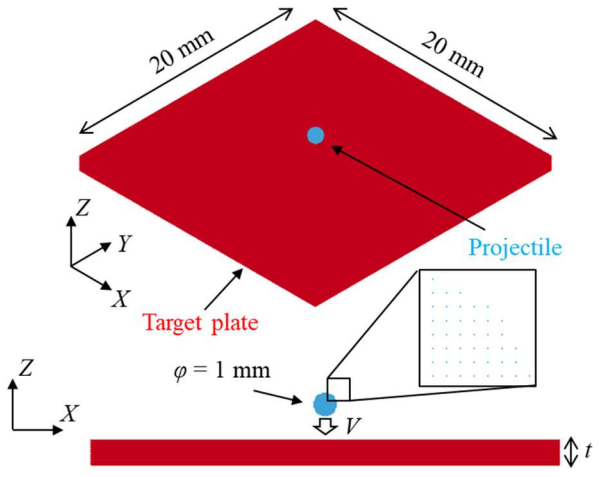

Figure 1. Overview of the numerical model.

The yield stress is expressed in the following Eq. 1.

$$\begin{aligned} \sigma_Y &= \left[A + B\left(\varepsilon^p_{eff}\right)^N\right](1 + C\,ln\,\dot{\varepsilon})[1 \\ &\quad - (T_H)^M] \\ \dot{\varepsilon} &= \frac{\dot{\varepsilon}^p_{eff}}{\dot{\varepsilon}_0} \\ T_H &= \frac{T - T_R}{T_M - T_R} \end{aligned} \tag{1}$$

Where ε^p_{eff} is the equivalent plastic strain, $\dot{\varepsilon}_0$ is the reference strain rate, T_M is the melting temperature, and T_R is the room temperature. A, B, C, and M are material constants and summarized in Tab. 2, referring to previous studies[4, 6]. The fracture strain is defined as follows.

$$\begin{aligned} \varepsilon^F &= \left(D_1 + D_2 \exp\left(D_3 \frac{\sigma_m}{\sigma_{eff}}\right)\right)(1 \\ &\quad + D_4 \ln \dot{\varepsilon})[1 + D_5 T_H] \\ D &= \sum \frac{\Delta \varepsilon^p_{eff}}{\varepsilon^F} \end{aligned} \tag{2}$$

ε^F is the fracture strain, σ_{eff} is the effective stress, σ_m is the hydrostatic stress, and fracture occurs when $D = 1$. D_1, D_2, D_3, D_4, D_5 are material constants.

With reference to previous studies, the linear multinomial equation of state was applied to A6061-T6, and the Mie-Grüneisen equation of state was applied to A2024-T3. The linear multinomial equation of state is defined as Eq. 3.

$$\begin{aligned} P &= C_0 + C_1\mu + C_2\mu^2 + C_3\mu^3 \\ &\quad + (C_4 + C_5 + C_6\mu^2)E_0 \\ \mu &= \frac{\rho}{\rho_0} - 1 \end{aligned} \tag{3}$$

Where P is pressure, ρ is current density, ρ_0 is initial density, and E_0 is initial internal energy. As reference [7], $C_0 = C_5 = C_6 = E_0 = 0$, $C_1 = 74.2$, $C_2 = 60.5$, $C_3 = 36.5$, $C_4 = 1.96$ were used for A6061-T6. The Mie-Grüneisen equation of state is the following Eq. 4.

$$\begin{aligned} P &= \frac{\rho_0 G^2 \mu}{[1 - (s-1)\mu]^2}\left[1 + \left(1 - \frac{\Gamma_0}{2}\right)\mu \right. \\ &\quad \left. - \frac{a}{2}\mu^2\right] + (\Gamma_0 + a\mu)E_0 \end{aligned} \tag{4}$$

From the previous study [4], we used $G = 5240$, $\Gamma_0 = 1.97$, $s = 1400$, $a = 0.48$ for A2024-T3.

We evaluated quantitatively target crater, ejecta mass, debris cloud, witness plate (WP) ejecta diameter, WP ejecta distribution. In the numerical simulation, the ejecta mass was obtained by counting the scattered

particles and multiplying the number of scattered particles by the mass per target particle. As for the status of the ejecta on WP, not all particles reach the WP 50 mm away within the calculation time. Therefore, the subsequent motion at WP was predicted by linear extrapolation from the behavior of the particles within the computation time. Additionally, we attempted to reproduce the size of impact traces on WP by assuming that particles distributed within a certain threshold circle are attached. In reality, the ejecta is scattered as large fragments, but in the analysis, it is represented as a collection of fine particles. Therefore, instead of plotting the smallest particles as they are, multiple particles in the vicinity (5 mm radius circle) are considered as one fragment. The position and size of a new particle were determined from the average position of the particles and the number of particles in the vicinity. The ejecta size obtained here is the predicted size of the ejecta itself. However, it is necessary to convert the ejecta size into the size of the impact scar and plot it to compare with the test results. We performed the collision analysis on an aluminum projectile with an average ejecta diameter and an average ejector velocity to copper WP, and we confirmed that the collision scar was approximately twice the ejecta diameter, so the collision scar diameter was calculated to be twice the ejecta diameter for the present analysis. Figure 2 shows these processes.

Table 1. Material properties of aluminum

Property	A6061-T6	A2024-T3
Density: ρ [g/cm^3]	2.70	2.78
Young's modulus: E [GPa]	68.9	73.1
Poisson's ratio: v	0.33	0.33
Specific heat capacity: c_p [J/g·K]	0.896	0.875
Thermal conductivity: λ [W/m·K]	167	121
Melting temperature: T_M [°C]	617	570

Table 2. Johnson-Cook parameters

Property	A6061-T6	A2024-T3
A [MPa]	324.1	167
B [MPa]	113.8	684
N	0.42	0.551
C	0.002	0.00
M	1.3	0.859
D_1	-0.77	0.112
D_2	1.45	0.123
D_3	-0.47	1.5
D_4	0.0	0.007
D_5	1.6	0.0

3 COLLISION TEST

The collision test was performed using two-stage light gas guns in the Hypervelocity Impact Facility of ISAS, JAXA, and Kurosawa laboratory, Kobe University. As an example, Fig. 3 shows the configuration of Kurosawa laboratory's two-stage light gas gun [8]. JAXA's light gas gun setup also follows Fig. 3. The two-stage light gas gun consists of three main processes: combustion of gunpowder in the ignition chamber, compression of light gas by the piston in the pump tube, and acceleration of the projectile in the launch tube. The impact velocity was measured in the velocimetry section by the laser cutting method. The collision zone consists of three plates, from left to right: the front side WP, the target, and the rear side WP. The ejecta generated by the impact of the projectile on the target collide with the front and rear WPs, forming impact scars. The distribution, amount, and size of ejecta were measured by observing the impact traces on WPs. The target was a 50 × 50 × t mm aluminum plate, and the WPs were 100 × 100 (sufficiently thick) copper plates. The WPs were completely fixed with a jig, and the target was fixed with a string so that the four corners were pulled in a 45° direction.

We observed the crater shape of the target after impact and the distribution of ejecta impact scars on the WPs by a digital microscope and measured the target loss mass as the amount of generated ejecta using an electronic scale. In the collision tests, ejecta mass was defined as follows.

$$m_{\text{ejecta}} = (m_{\text{target\_before}} + m_{\text{projectile\_before}}) - m_{\text{target\_after}} \quad (5)$$

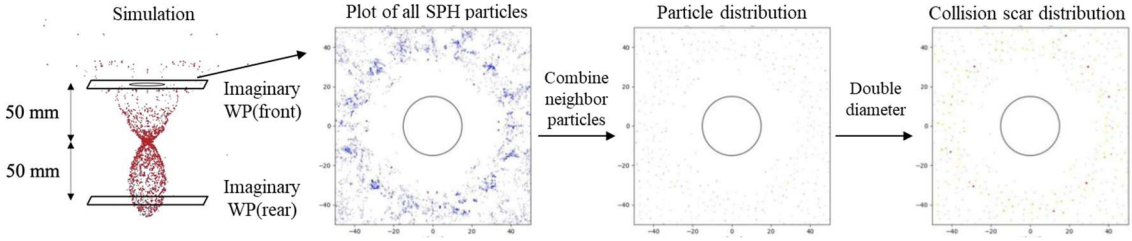

Figure 2. Predictive processing of ejecta collision scars on WP in simulation for comparison to the collision test.

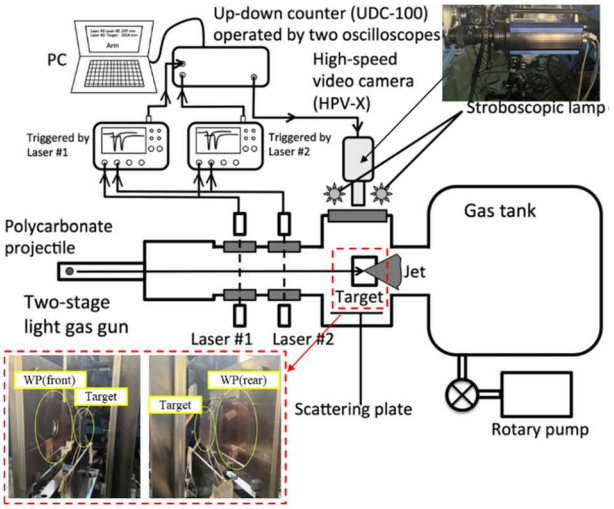

Figure 3. Collision test setup with two-stage gas gun [8].

4 RESULTS AND DISCUSSION

Examples of debris clouds obtained in the collision test with the high-speed camera and in the simulation are shown in Fig. 4. The debris cloud shapes are well reproduced. The approximate debris velocity can also be calculated from the high-speed camera, and it was confirmed that the results are close to the simulation results.

The target after testing at V = 3 km/s and t = 1 mm is shown in Fig. 5. Under these conditions, the projectile penetrated the target in both the test and analysis. A cross-section of the crater was extracted from the scan data for comparison with the analysis. In the case of penetration, it can be seen that the rear side of the crater is also significantly deformed. For ease of comparison, we define the crater diameter φ as the distance between the ridges of the craters on the front side. The crater diameters obtained from the test and analysis are shown in Fig. 6. The diameters of the frontal craters agree with a high degree of accuracy, with the average relative error between the experiment and the numerical analysis being about 6 %. However, details of the crater cross section show differences in the diameter of the rear crater and the shape of the crater ridge.

Next, a comparison of the total ejector volume on the front and rear sides is shown in Fig. 7. The analytical value of V = 5 km/s and t = 2mm is much larger than the experimental value because a large number of particles are generated on the rear side due to penetration while the experimental value is non-penetrating. However, the other values are considered to be roughly estimated. Next, we evaluated the size of the ejecta. Since direct measurement was not possible in the experiment, the maximum diameters of the impact traces are compared here from the WP impact traces.

A comparison of the results for the front side ejector is shown in Fig. 8. The error is larger than the crater diameter, and overall, the analysis is 10~20% larger than the experiment. However, the trends with respect to plate thickness and impact velocity are generally consistent.

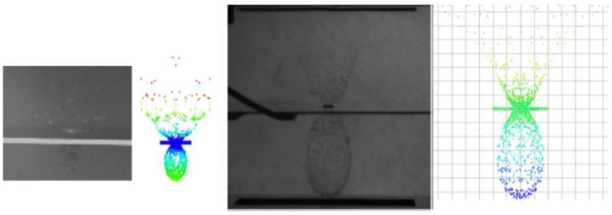

Figure 4. Comparison of debris cloud between collision test and simulation (left: V = 3 km/s, t = 1mm, right: V = 7km/s, t = 1mm). The colors in the simulation results show the ejecta velocity.

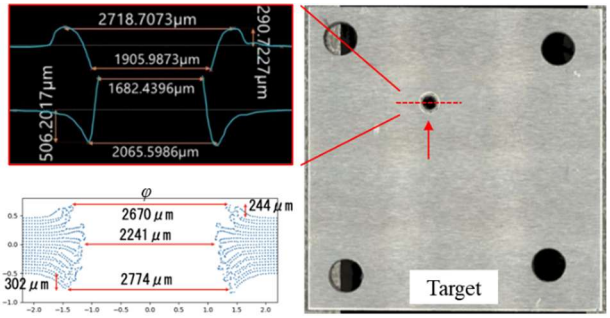

Figure 5. Cross-section of target crater of collision test (upper left) and simulation (lower left).

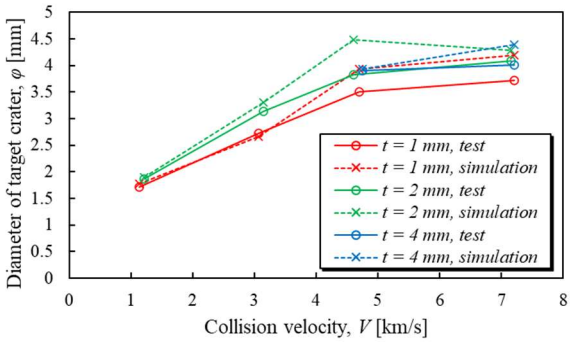

Figure 6. Comparison of diameter of target crater between collision test and simulation.

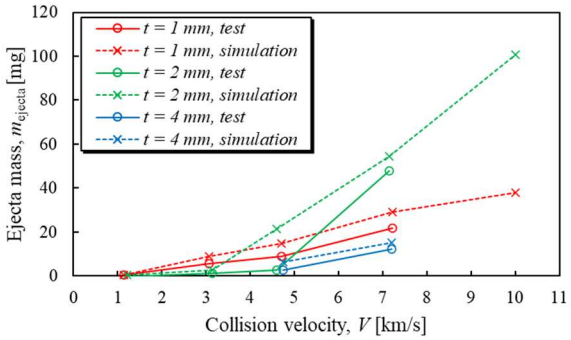

Figure 7. Comparison of ejecta mass between collision test and simulation.

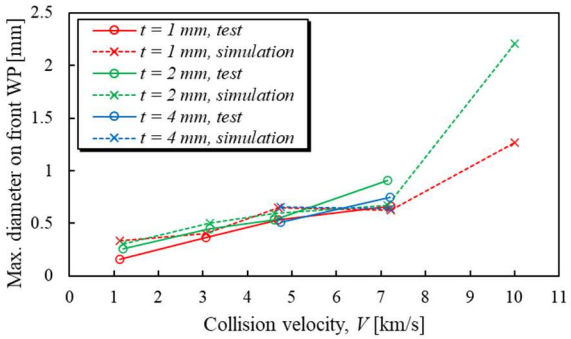

Figure 8. Comparison of maximum scar diameter on front WP between collision test and simulation.

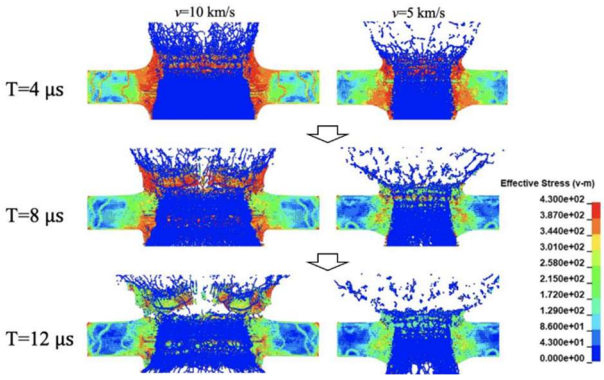

Figure 9. Debris cloud and effective stress distribution in the simulation (left: V = 10 km/s, t = 2mm, right: V = 5 km/s, t = 2mm).

The above study confirms that the established numerical model can reproduce the behavior of ejecta caused by high-velocity collisions and can quantitatively predict it. Then, we tried to predict ejecta behavior at 10 km/s, where experiments are impossible.

In the 10 km/s collision, some very large ejecta were observed, which were not seen in collisions below 7 km/s. Fig. 8 shows the deformation and stress distribution at 10 km/s and 5 km/s immediately after the collision. At 10 km/s, the target plate is greatly deformed due to the large impact energy, and a high crater is formed on the front side (see the red part of the figure). The target is observed to be broken off near the base as a result of the high stress applied near the uplifted area, and the target is dispersed as a large ejecta as if it were peeled off. The ejecta mass and maximum diameter of ejecta predicted by the suggested model for a 10 km/s collision are appended in Fig. 7 and 8, respectively. The ejecta mass depends on the collision velocity and target thickness and positively correlates with these. Below 7 km/s, the maximum ejecta diameter did not change with target thickness, whereas at 10 km/s, the larger the target thickness, the larger the ejecta. This is due to the front spall-like dispersal behavior shown in Fig. 9.

5 CONCLUSION

In this study, we constructed a numerical model between an aluminum projectile and target plate simulating space debris collision using the SPH method and predicted the ejecta scattering behavior at ultra-high velocities based on comparison with collision tests.

A comparison with the collision tests showed that the crater diameter matched with high accuracy. The trends of increase in the maximum scar diameter on WP and the amount of ejecta generated were also very similar, confirming that the phenomenon was generally reproduced.

Based on the results, we predicted the amount of ejecta generated and the maximum ejector diameter at 10 km/s. It was also confirmed that large ejecta, which do not occur in the experimentally feasible velocity range, are generated in this velocity. Since large ejecta have large kinetic energy and lead to catastrophic destruction of the satellite and the release of a large amount of ejecta, it is considered important to evaluate such ejecta that cannot be confirmed by collision tests in the high-speed region through numerical analysis.

As a future work, we will establish the numerical model of the Carbon Fiber Reinforced Plastic (CFRP) target plate to predict its ejecta.

ACKNOWLEDGMENT

The research results were obtained using the Hypervelocity Impact Facility (former name: Space Plasma Laboratory) of ISAS, JAXA.

REFERENCES

1. C. Wiedemann, et al., “Modeling the Space Debris Environment – Latest Improvements and Updates”, Proceedings of the 9th Space Debris Workshop, 2021.
2. NASA, “Orbital Debris Quarterly News”, Vol.29, Issue.1, 2025.
3. W. Schill, J. V. Wasem and J. M. Owen, “Modelling and simulation of cratering and ejecta production during high velocity impacts”, Journal of Dynamic Behavior of Materials, 3.2, 180-188, 2017.
4. L. E. Schwer and C. A. Windsor, “Aluminum plate perforation: a comparative case study using Lagrange with erosion, multi-material ALE, and smooth particle hydrodynamics”, 7th European LS-DYNA conference, Vol. 28, 2009.
5. G.R.Johnson, W.H.Cook, “Fracture Characteristics of Metals Subjected to Various Strains, Strain Rates, Temperatures and Pressures”, Engineering Fracture Mechanics Vol.21, No.1, 31-48, 1985.
6. K.Fowler and F.Teixeira-Dias, “Hybrid Shielding for Hypervelocity Impact of Orbital Debris on Unmanned Spacecraft”, applied sciences, 2022, 12, 7071.
7. K. Vahedi and N. Khazraiyan, “Numerical Modeling of Ballistic Penetration of Long Rods into Ceramic/Metal Armors”, 8th European LS-DYNA conference, 2011.
8. Kurosawa, K., Nagaoka, Y., Senshu, H., Wada, K., Hasegawa, S., Sugita, S., and Matsui, T., “Dynamics of Hypervelocity Jetting during Oblique Impacts of Spherical Projectiles Investigated via Ultrafast Imaging: ULTRAFAST IMAGING OF IMPACT Jetting,” Journal of Geophysical Research: Planets, Vol. 120, No. 7, 2015, pp. 1237–1251.